

Structure-Based Screening to Discover New Inhibitors for Papain-like Proteinase of SARS-CoV-2: An *In Silico* Study

Mostafa Jamalana,* Ebrahim Barzegari, and Fathollah Gholami-Borujeni



Cite This: *J. Proteome Res.* 2021, 20, 1015–1026



Read Online

ACCESS |



Metrics & More



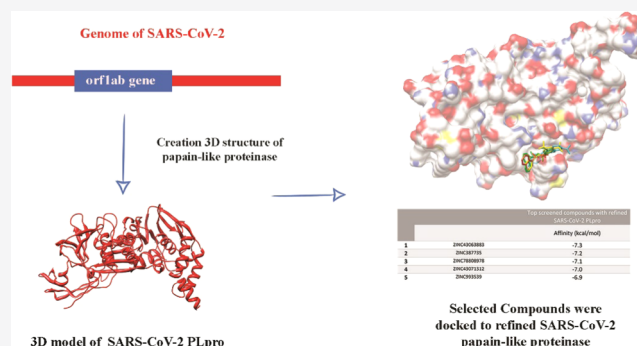
Article Recommendations



Supporting Information

ABSTRACT: Severe acute respiratory syndrome coronavirus 2 (SARS-CoV-2) expresses a multifunctional papain-like proteinase (PLpro), which mediates the processing of the viral replicase polyprotein. Inhibition of PLpro has been shown to suppress the viral replication. This study aimed to explore new anti-PLpro candidates by applying virtual screening based on GRL0617, a known PLpro inhibitor of SARS coronavirus (SARS-CoV). The three-dimensional (3D) structure of SARS-CoV-2 PLpro was built by homology modeling, using SARS-CoV PLpro as the template. The model was refined and studied through molecular dynamic simulation. AutoDock Vina was then used to perform virtual screening where 50 chemicals with at least 65% similarity to GRL0617 were docked with the optimized SARS-CoV-2 PLpro. In this screening, 5-(aminomethyl)-2-methyl-*N*-[(1*R*)-1-naphthalen-1-ylethyl]benzamide outperformed GRL0617 in terms of binding affinity (−9.7 kcal/mol). Furthermore, 2-(4-fluorobenzyl)-5-nitro-1*H*-isindole-1,3(2*H*)-dione (previously introduced as an inhibitor of cyclooxygenase-2), 3-nitro-*N*-[(1*r*)-1-phenylethyl]-5-(trifluoromethyl)benzamide (inhibitor against *Mycobacterium tuberculosis*), as well as the recently introduced SARS-CoV-2 PLpro inhibitor 5-acetamido-2-methyl-*N*-[(1*S*)-1-naphthalen-1-ylethyl]benzamide showed promising affinity for the viral proteinase. All of the identified compounds demonstrated an acceptable pharmacokinetic profile. In conclusion, our findings represent rediscovery of analgesic, anti-inflammatory, antibacterial, or antiviral drugs as promising pharmaceutical candidates against the ongoing coronavirus.

KEYWORDS: SARS-CoV-2, papain-like proteinase, inhibitor, protein modeling, virtual screening, docking



1. INTRODUCTION

The severe acute respiratory syndrome coronavirus 2 (SARS-CoV-2)-associated disease (COVID-19) that emerged in Wuhan, China, at the end of 2019 has led to a global outbreak and now is a major public health issue.¹ The pneumonic spillover was declared as a global pandemic on March 11, 2020.² By December 3, 2020, data from World Health Organization (WHO) have shown over 64.5 million cases and more than 1.49 million deaths caused by COVID-19 worldwide. According to CDC reports, the virus is thought to spread mainly person-to-person or through contact with surfaces contaminated with respiratory droplets produced when an infected person coughs or sneezes.³ The highly transmissible nature of the virus demands urgent consideration of developing specific and effective drugs to handle the circulating infection. Virtual screening as applied in computer-aided drug design is an appropriate approach to accelerate the identification of efficient medicines against SARS-CoV-2.⁴ In this approach, the data of the viral genome or protein structures are exploited in combination with existing pharmacological knowledge such as approved drugs and available synthesized chemicals, to discover potential compounds against desired targets.⁴

Consensus genome of SARS-CoV-2 has ~80% similarity with previously sequenced severe acute respiratory syndrome coronavirus (SARS-CoV) genome. Replicase polyprotein 1ab (pp1ab) in SARS-CoV is a multifunctional protein with vital roles in transcription and replication of viral RNAs.⁵ The polyprotein gene (orf1ab) encodes several nonstructural protein (nsp) products, including nsp3, or papain-like proteinase (PLpro), a proteinase responsible for the cleavage of the translated viral replicase polyprotein.⁶ SARS-CoV PLpro is also involved in the virally induced cytoplasmic assembly of double-membrane vesicles and demonstrates other activities such as deubiquitination and deISGylation for processing polyubiquitin chains.⁷ Many previous studies have shown that inhibition of SARS-CoV PLpro could efficiently inhibit the viral infection.^{7b,8} The compound GRL0617 (5-amino-2-methyl-*N*-[(1*R*)-1-naph-

Received: October 27, 2020

Published: December 22, 2020



thalen-1-ylethyl]benzamide) has been reported as one of the most efficient inhibitory ligands against SARS-CoV PLpro.^{8b} The present paper reports the application of molecular modeling and virtual screening based on GRL0617 to identify novel compounds against SARS-CoV-2 PLpro. The screening approach taken here confirmed a recent experimentally identified inhibitor and introduced novel potential promising compounds for suppressing the replication of the novel coronavirus.

2. MATERIALS AND METHODS

2.1. *In Silico* Mutagenesis

At the first step, the amino acid sequences of pp1ab polypeptide from SARS-CoV (NCBI Reference Sequence: NC_004718.3) and from SARS-CoV-2 (NCBI Reference Sequence: NC_045512.2) were retrieved from NCBI Nucleotide Database. Binary sequence alignment was performed using Clustal Omega tool to compare the sequences to identify the sequence positions similar or differing between the two orthologous proteins.⁹ In the subsequent step, crystallographically determined structure of SARS-CoV papain-like proteinase/deubiquitinase bound to GRL0617 as an inhibitor molecule was retrieved from <https://www.rcsb.org> (PDB ID: 3E9S).^{8b} The identified differing residues in PLpro from SARS-CoV were then mutated to their corresponding residues in SARS-CoV-2 papain-like proteinase, using a rotamer function of UCSF Chimera.¹⁰ For each mutated residue, we chose the lowest CHI number in Dunbrack backbone-dependent rotamer library.¹⁰

2.2. Molecular Dynamic Refinement of SARS-CoV and SARS-CoV-2 PLpro Structural Models

Both the experimental structure of SARS-CoV PLpro and the newly created model of SARS-CoV-2 PLpro underwent MD simulation procedures, to obtain optimized models and to improve our understanding about SARS-CoV-2 PLpro. Simulations and analyses of produced trajectories were performed using Gromacs (version 4.5.5) software package.¹¹ HET atoms were removed from the 3E9S structure, and topologies were defined using OPLS-AA force field. The SARS-CoV PLpro/deubiquitinase domain and the generated SARS-CoV-2 PLpro coordinates were located in separate cubic boxes, solvated by SPC216 model for the water molecule, and neutralized by the addition of a sufficient number of Cl⁻ ions. After all of the indicated steps, the solvated and neutralized structures were energy-minimized by steepest descent algorithm until the maximum force <1000.0 kJ/(mol nm) was reached. These geometrically optimized structures were used as the ligand-binding target in the structure-based virtual screening as described in Section 2.4. We implemented the same protocol for producing minimized and neutralized three-dimensional (3D) model of SARS-CoV PLpro/deubiquitinase domain and SARS-CoV-2 PLpro where the topologies were determined by GROMOS96-43a1 force field. The structures were subjected to 100 ps of MD simulations in the canonical (NVT) ensemble to increase the temperature of the systems to 298 K. After 200 ps of MD equilibration in the isothermal–isobaric (NPT) ensemble, the final equilibrated structures were used to carry out 35 ns MD simulations. The particle-mesh Ewald algorithm was used to account for long-range electrostatic interactions.¹² This MD refinement step provided initial geometries for verifying the best-binding compounds identified through the screening procedures.

2.3. Virtual Screening of Compounds with High Similarity to GRL0617

In this study, chemical structures with high similarity to GRL0617 were searched in BindingDB (<http://www.bindingdb.org>). We retrieved 50 chemical agents with at least 65% similarity to the input compound. The compounds were ranked according to the maximum Tanimoto similarity of each compound to any of the items in a set of active compounds used for training the search method.¹³

2.4. Screening Based on Targeted Binding

Before performing the structure-based virtual screening through molecular docking experiments, we implemented an internal validation phase, where GRL0617 was docked against the PDB model of SARS-CoV PLpro/deubiquitinase domain. AutoDock Vina¹⁴ was used for automated docking to find the lowest-energy poses of the small molecule against SARS-CoV PLpro. We used AutoDock Tools 4.2 software for determination of grids and converting of files formats.¹⁵ The chemical structures identified in the ligand search step were docked against the generated minimized SARS-CoV-2 PLpro structure according to a grid set based on coordinates of GRL0617 in the experimental model of SARS-CoV PLpro/deubiquitinase domain. Five compounds with the lowest energy of binding to SARS-CoV-2 PLpro were docked against the refined protein structure and analyzed in terms of molecular interaction and mechanism. As an additional validation for the binding energy comparison among the chemical compounds, we set up and carried out dockings of top compounds using SwissDock and applying the default parameters.¹⁶ For visualizing protein structures, depicting the protein–ligand interactions, and rendering of images, we used VMD,¹⁷ Pymol,¹⁸ LIGPLOT,¹⁹ and UCSF Chimera programs,¹⁰ as well as ENDscript 2 server-based tools.²⁰

2.5. Pharmacokinetic and Toxicity Properties of Top Compounds

Physicochemical properties of selected compounds with the highest affinity for SARS-CoV-2 PLpro were determined by ChemSpider database²¹ and SwissADME.²² Toxicity of compounds was predicted by vNN-ADMET web server.²³

3. RESULTS AND DISCUSSION

3.1. Preparing the Structural Model of Papain-like Proteinase Domain from SARS-CoV-2

Sequence homology between proteins implies similarity between their structures, which may also follow an identical biological function of two proteins. Functional similarity between orthologous proteins from evolutionary-related species is even more established, and it indicates high conservation in functionally critical sites. Differential residues between such proteins typically locate in positions with limited or no functional importance. This provides a rationale for the use of an experimentally determined structure as a valid tool to build the model of its orthologue. We applied *in silico* mutagenesis for this purpose.

Based on the available genomic sequence of SARS-CoV-2 isolate Wuhan-Hu-1 (<https://www.ncbi.nlm.nih.gov/nuccore/1798174254>), the viral genome is shown to be ~80% similar to that of SARS-CoV (<https://www.ncbi.nlm.nih.gov/nuccore/30271926>). Expressed orf1ab polyprotein (pp1ab) of SARS-CoV-2 has 91.7% similarity (including 85.4% identical positions) to that of SARS-CoV. Both virus species encode PLpro as a conserved domain in the final gene product. The

SARS-CoV	SDDTLRSEAFEYHYHTLDESFLGRYMSALNHTKKWKFPQVGGLTSIKWADNNCYLSSVLLA	60
SARS-CoV-2	SDDTLRVSEAFEYHYHTDPSFLGRYMSALNHTKKWKYPQVNGLTSIKWADNNCYLATALLT	60
	***** ***** * *****:***:*****:..**:	
SARS-CoV	LQQLEVKFNAPALQEAYYRARGDAANFCALILAYSNKTVGELGDVRETMTHLLQHANLE	120
SARS-CoV-2	LQQIELKFNPPALQDAYYRARGAANFCALILAYCNKTVGELGDVRETMSYLFQHANLD	120
	: *****:*****:*****:***:*****:..**:	
SARS-CoV	SAKRVLNVVCKHCGQKTTTLTGVEAVMYMGTLSDYDNLKTVGSIPCVCGRDATQYLVQQES	180
SARS-CoV-2	SAKRVLNVVCKTCGQQTTTLTGVEAVMYMGTLSEYQFKKGVQIPCTCGKQATKYLVQQES	180
	* ***** ***: ***:*****:..**:* ***:**:* *****	
SARS-CoV	SFVMSAPPAEYKLGQGTFLCANEYTGNYQCQGHYTHITAKETLYRIDGAHLTKMSEYKGP	240
SARS-CoV-2	PFVMSAPPAQYELKHGTFTCASEYTGNYQCQGHYKHITSKETLYCIDGALLTKSSEYKGP	240
	*****:***:*** ***:*****:***:***** ***:**:* *****	
SARS-CoV	VTDVFKETSYYTTI 255	
SARS-CoV-2	ITDVFYKENSYYTTI 255	
	:*****:*****	

Figure 1. Pairwise sequence alignment of papain-like proteinase from SARS-CoV versus that from SARS-CoV-2. Identical amino acids were marked by asterisks, and similar amino acids were marked by dots.

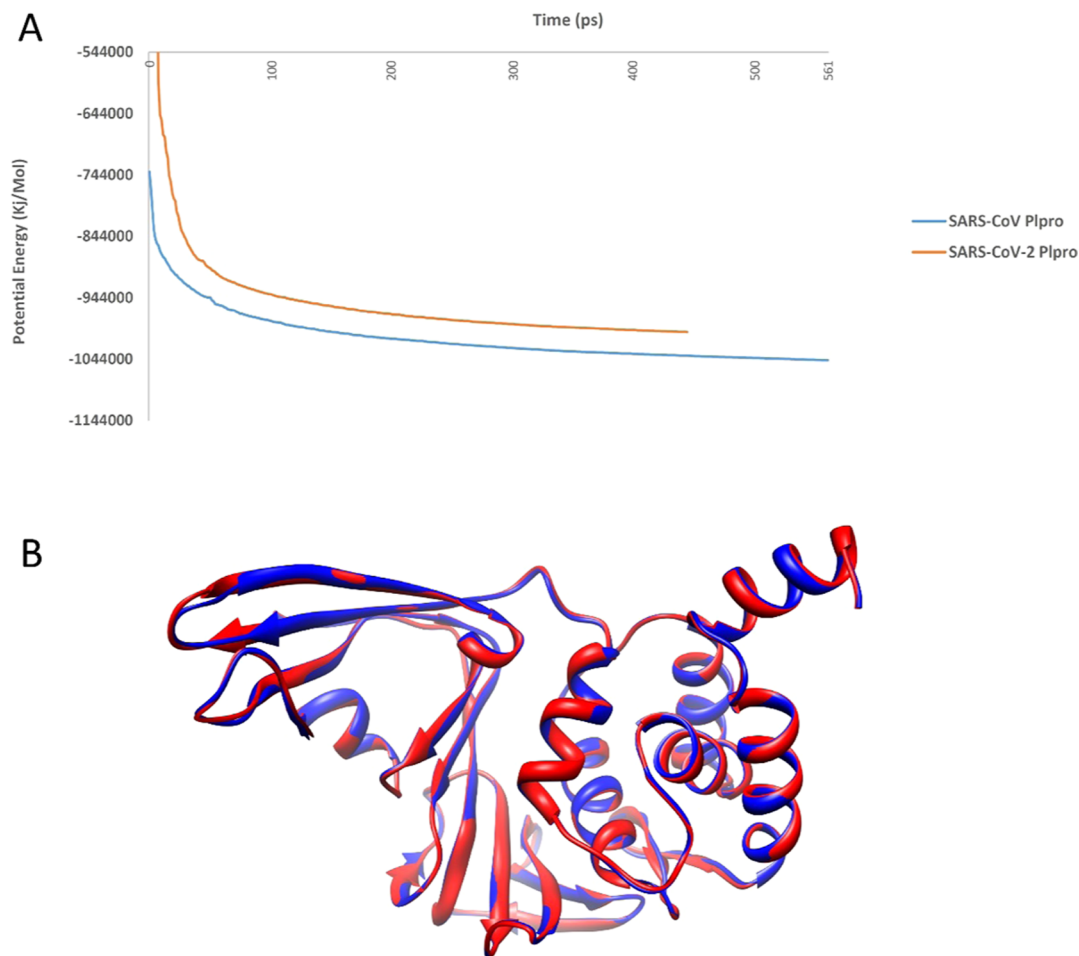


Figure 2. (A) Energy minimization graph for papain-like proteinase from SARS-CoV (3E9S PDB entry: blue) and papain-like protease from SARS-CoV-2 (SARS-CoV-2 PLpro: red). (B) Superimposition of the experimental model of SARS-CoV PLpro (blue) and the final minimized SARS-CoV-2 PLpro structural model (red).

sequence similarity between PLpro/deubiquitinase domains from SARS-CoV and SARS-CoV-2 is 84.9% (including 75.0% identical positions). In this study, we took up the experimentally determined PLpro/deubiquitinase domain of nsp3 protein (256 residues) and replaced those amino acids differing from SARS-CoV PLpro with their corresponding residues in SARS-CoV-2

PLpro (Figure 1). Fifty-two positions underwent *in silico* mutagenesis to create the SARS-CoV-2 PLpro model. This primary model was minimized to reach the lowest energy level and finest possible coordinates (Figure 2A). Minimized structures of PLpro from SARS-CoV and SARS-CoV-2 were superimposed, showing a significant spatial fit (Figure 2B). In

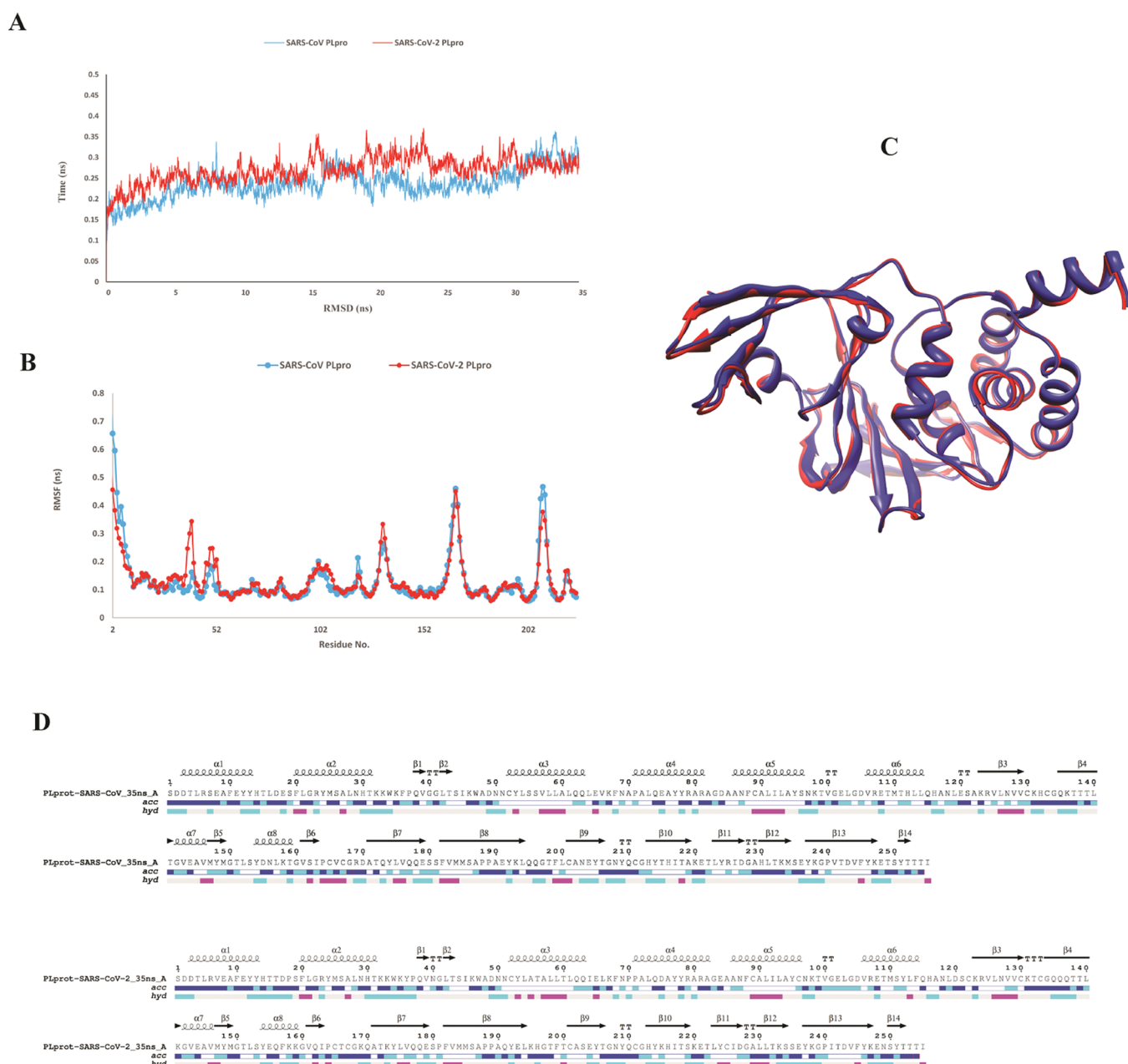


Figure 3. (A) Root-mean-squared deviation (RMSD) of papain-like protease from SARS-CoV (blue) and SARS-CoV-2 (red) during 35 ns of molecular dynamic simulation. (B) Root-mean-squared fluctuations (RMSF) of papain-like protease from SARS-CoV (blue) and SARS-CoV-2 (red) during 35 ns of molecular dynamic simulation. (C) Superimposition of the 3D structure of SARS-CoV PLpro (blue) and SARS-CoV-2 PLpro (red) after 35 ns of MD simulation. (D) Secondary structures of PLpro from SARS-CoV and SARS-CoV-2 after 35 ns of MD simulation.

the next step, the minimized model was refined by molecular dynamic simulation.

3.2. MD Simulation of SARS-CoV PLpro and SARS-CoV-2 PLpro Structures

A structural model produced through *in silico* mutagenesis would require to be optimized both locally and globally. Energy minimization (EM) methods can be used to remove local residue clash, and molecular dynamic simulations help refine the global structure. The advantage provided by MD simulations is the ability to study the dynamics inherent in structural models, a feature that is not integrated in any molecular docking setup. The dynamic implementation allows us to release geometrical strains in the protein conformation. We employed both EM and

MD techniques to reach an optimized structure for SARS-CoV-2 PLpro.

The 3D structure of SARS-CoV PLpro from 3E9S PDB coordinate and the generated model of SARS-CoV-2 PLpro were solvated in a simulation water box and energy-minimized, followed by a production dynamic simulation for 35 ns. Based on the obtained root-mean-squared deviation (RMSD) graph (Figure 3A), both structures reached their stable coordinates after almost 15 ns of the simulation process. The average RMSD values for the PLpro structure of SARS-CoV and SARS-CoV-2 were 0.2701 and 0.2380 nm, respectively, which demonstrates the stability and validity of the constructed model for SARS-CoV-2 PLpro (Figure 3A). A comparative analysis of the 3D structure of SARS-CoV PLpro and SARS-CoV-2 PLpro (Figure

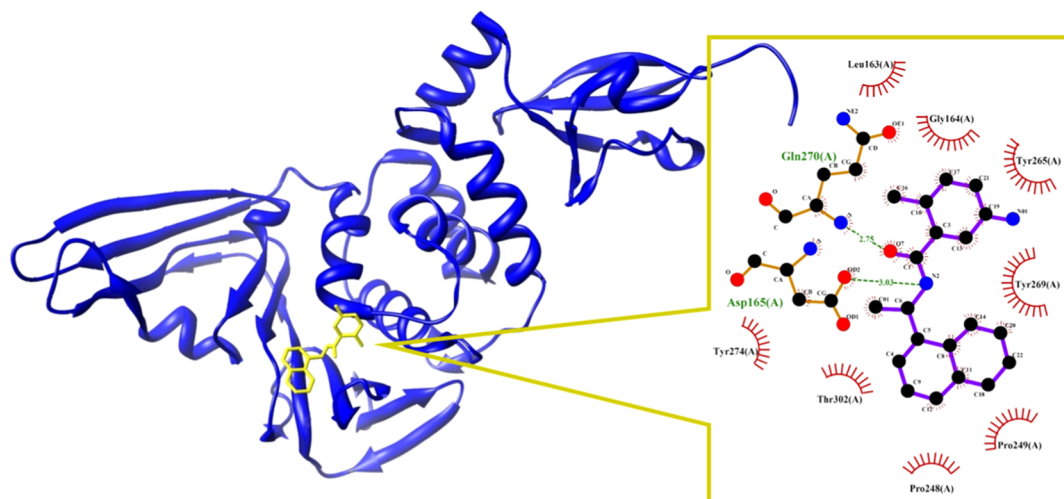


Figure 4. Interaction of SARS-CoV papain-like proteinase with GRL0617 as indicated by the X-ray crystallographic model (3E9S PDB entry) and two-dimensional (2D) illustration of the interactions between SARS-CoV PLpro and GRL0617.

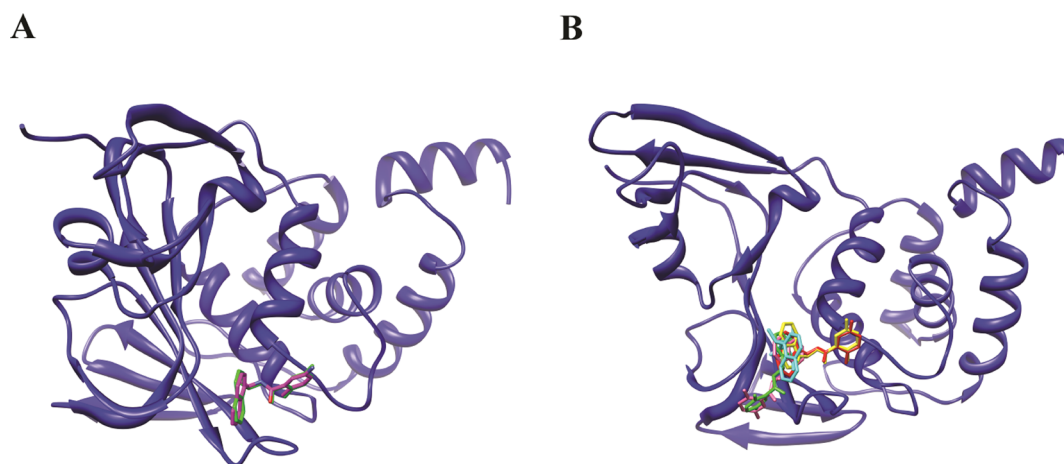


Figure 5. (A) GRL0617 ligand accommodated in its specific binding cavity on the experimental PDB model of SARS-CoV PLpro (purple sticks) and the same ligand docked into SARS-CoV PLpro (green sticks). (B) Conformations of GRL0617 as docked into SARS-CoV PLpro with different binding energies: red (9.6 kcal/mol), yellow (-9.0 kcal/mol), green (-7.1 kcal/mol), cyan (-7.0 kcal/mol), and pink (-6.7 kcal/mol).

Table 1. Binding Data for Five Best Poses of GRL0617 against SARS-CoV PLpro and SARS-CoV-2 PLpro, as Obtained by Two Different Docking Tools

	GRL0617 with SARS-CoV PLpro (kcal/mol)			GRL0617 with SARS-CoV-2 PLpro (kcal/mol)		
	affinity (Vina)	estimated ΔG (SwissDock)	FullFitness (SwissDock)	affinity (Vina)	estimated ΔG (SwissDock)	FullFitness (SwissDock)
1	-9.6	-8.16	-1221.03	-7.5	-7.06	-1242.76
2	-9.0	-8.12	-1219.84	-7.4	-7.08	-1242.76
3	-7.1	-7.92	-1219.04	-7.0	-7.07	-1249.97
4	-7.0	-7.91	-1218.96	-7.0	-7.07	-1235.49
5	-6.7	-7.61	-1213.43	-6.8	-7.07	-1235.66

3C) and their secondary structures (Figure 3D) after 35 ns of the simulation process did not show any significant variation between the two structural models. As shown in Figure 3C, much similarity is observed in 3D structures of SARS-CoV PLpro and SARS-CoV-2 PLpro after 35 ns of MD simulation. This kind of similarity could be used for designing inhibitors against SARS-CoV-2 PLpro based on the structures of previously introduced inhibitors for SARS-CoV PLpro. But, in the way of identifying the new inhibitors, differences such the turn composed of residues 131–133 of SARS-CoV-2 PLpro,

which was not seen in the SARS-CoV PLpro structure after 35 ns of MD simulation, should also be considered (Figure 3D).

In addition, root-mean-squared fluctuations (RMSF) of Ca' s for the two protein models during the simulation process (Figure 3B) confirmed the similar patterns of residue dynamics along the sequence of the two orthologous proteins. The identical behavior of SARS-CoV PLpro and SARS-CoV-2 PLpro during the simulation process could support the notion that previously reported inhibitors of SARS-CoV PLpro may be exploited as inhibitors against SARS-CoV-2 PLpro activity. The improved simulated model of SARS-CoV-2 PLpro could be

utilized for virtual screening to achieve most potent and specific inhibitors that inhibit proteolytic activity of SARS-CoV-2 PLpro.

3.3. Docking Experiment Validation

The crystallographic model of SARS-CoV PLpro encompasses the inhibitor GRL0617 bound to the proteinase active site (Figure 4). Based on previous reports, IC_{50} for inhibition of SARS-CoV PLpro activity by GRL0617 is 230 nM.²⁴ We utilized this protein–ligand complex for performing a validation phase to confirm the docking process. GRL0617 was docked against SARS-CoV PLpro (Figure 5A), resulting in -9.6 kcal/mol as the lowest binding energy (Table 1). The binding energy data for the poses of GRL0617 in SARS-CoV PLpro active site were also confirmed by SwissDock results (Table 1). Interacting conformations of the compound are depicted in Figure 5B. GRL0617 with an affinity of -9.6 kcal/mol is exactly laid on its coordinate in the experimental PDB model (Figure 5A). In this pose, the naphthalene ring of GRL0617 is surrounded by a hydrophobic hole composed of Thr302, Pro248, Pro249, and Tyr269. The N2 and O7 atoms from GRL0617 make salt bridges with the O and N atoms from Asp165 and Gln270 from SARS-CoV PLpro, respectively (Figure 4).

GRL0617 was also docked against the SARS-CoV-2 PLpro structure (Table 1 and Figure 6). In the complex of SARS-CoV-

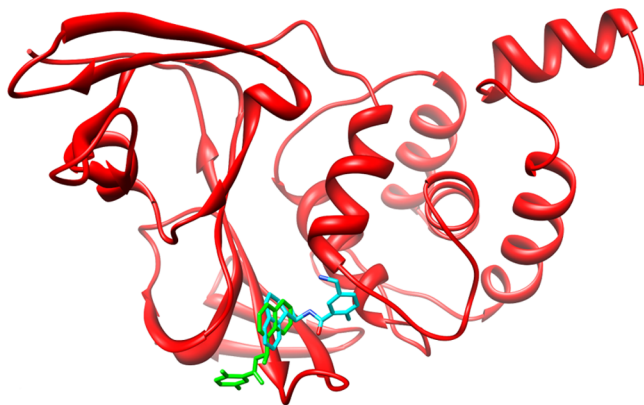


Figure 6. GRL0617 (cyan sticks) and ZINC43071312 (green sticks) in their most favorable conformations for binding to SARS-CoV-2 PLpro (binding energies of -7.5 and -9.7 kcal/mol, respectively).

2 PLpro with GRL0617, the conformation of the aniline ring of the ligand is different from that in the SARS-CoV PLpro PDB as the reference model (Figure 6). As shown in Table 1, -7.5 kcal/mol is the lowest ΔG of GRL0617 binding to SARS-CoV-2 PLpro. This value is more positive than -9.6 kcal/mol, as reported for SARS-CoV PLpro, showing that mutations inserted in SARS-CoV-2 PLpro could affect the affinity of binding for GRL0617. Independent validation of the docking by use of SwissDock also confirmed the binding energy results for the poses of GRL0617 in the SARS-CoV PLpro active site (Table 1). In the next step, the chemical structure of GRL0617 was used as a template for screening new inhibitors against SARS-CoV-2 PLpro.

3.4. Identification of New Potential Inhibitors for SARS-CoV-2 PLpro

As indicated in Section 2, GRL0617 was used as the baseline compound of the virtual screening to identify potential inhibitors against PLpro. To date, numerous protease inhibitors have been approved as drugs against viral species such as human

immunodeficiency virus and hepatitis C virus.²⁵ Though GRL0617 is not an approved medicine, it is a potent compound suggested to specifically inhibit the protease in SARS-CoV.^{8b} We chose GRL0617 as the baseline compound since, compared to the approved viral protease inhibitors, it may represent a more specific inhibitory profile against the protease of coronavirus family.

The top-20 chemical structures with the lowest binding affinity to the proteinase are listed in Table 2. Among these candidates, four compounds demonstrated lower ΔG of binding compared to GRL0617 to SARS-CoV-2 PLpro (≤ -7.5 kcal/mol) (Table 2). We performed the dockings for top-five compounds using SwissDock as an independent tool to validate the binding results. The data were in agreement with affinity values obtained from AutoDock Vina (Table 2).

The lowest binding energy (-9.7 kcal/mol) was observed for 5-(aminomethyl)-2-methyl-N-[(1R)-1-naphthalen-1-ylethyl]-benzamide (ZINC43071312). This compound has been shown to inhibit SARS-CoV PLpro activity with an IC_{50} of 460 nM.²⁴ Based on the interaction profile of the new compound, ZINC43071312 makes two salt bridges with Asp165 and Gln270 of SARS-CoV-2 PLpro. The naphthalene moiety of the compound is surrounded by a hydrophobic hole composed of Tyr269, Pro249, Thr302, Pro248, Tyr274, and Tyr265 (Figures 6 and 7A).

The compounds 2-(4-fluorobenzyl)-5-nitro-1H-isoindole-1,3(2H)-dione (ZINC993539), 3-nitro-N-[(1R)-1-phenylethyl]-5-(trifluoromethyl)benzamide (ZINC78808978), and 5-acetamido-2-methyl-N-[(1S)-1-naphthalen-1-ylethyl]-benzamide (ZINC387735) also showed favorable interactions with SARS-CoV-2 PLpro, with binding energies of -8.4 , -8.4 , and -7.6 kcal/mol, respectively (Table 2 and Figure 7).

The molecular interactions of five compounds demonstrating the highest affinity for SARS-CoV-2 PLpro were further studied through docking with the MD-refined PLpro structure. While the affinity values were shown to be smaller in this step (Tables 2 and 3), the compounds still have a considerable affinity for SARS-CoV-2 PLpro. Among the compounds docked to the refined structure of SARS-CoV-2 PLpro, ZINC43063883 showed the lowest value of binding energy (-7.3 kcal/mol; see Table 3). This compound forms two salt bridges with Gln210 and Tyr209 of SARS-CoV-2 PLpro and interacts with Pro189, Tyr205, and Tyr214 through its hydrophobic moieties and naphthalene and benzene rings (Figure 8). An independent validation docking by use of SwissDock showed ZINC43071312 as the best compound, which confirms the findings from structures before MD refinement (Table 3). The results of SwissDock showed contradiction with Vina in terms of the compound ranks. In tool benchmarking studies, this level of inconsistency of calculated affinities has been shown to be common and acceptable.²⁶ Due to its high accuracy and speed, Vina has been suggested as the preferred platform for screening,²⁶ as also applied in this study. Nevertheless, the observed contradiction emphasizes the requirement of wet-lab screening for all identified compounds to find the best candidate.

Although binding affinity and specificity are critical to have an efficient inhibitor, other properties such as solubility and ability to penetrate into cells via cellular membrane, low toxicity, gastrointestinal absorption for oral administration, and carcinogenic potential of the ligand are also important. Thus, physicochemical, biological, and cytotoxicity of screened compounds were investigated in the next step.

Table 2. Binding Affinity to SARS-CoV-2 PLpro for the Top-20 (Out of 50) Compounds with the Highest Structural Similarity to GRL0617^{4a}

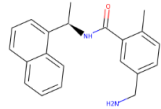
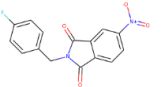
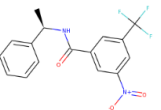
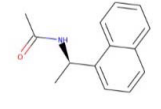
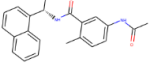
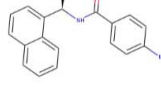
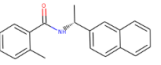
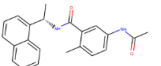
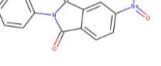
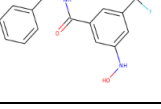
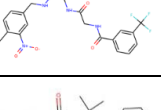

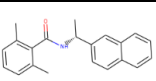
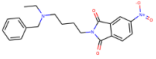
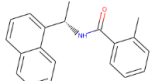
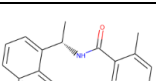
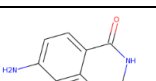
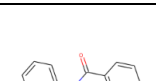
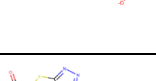

	ZINC ID	Chemical Structure	ACD/IUPAC Name	Affinity (kcal/mol)
1	ZINC43071312		5-(Aminomethyl)-2-methyl-N-[(1R)-1-(1-naphthyl)ethyl]benzamide	-9.7 $\Delta G = -9.52$ FF = -1274.87
2	ZINC993539		2-(4-Fluorobenzyl)-5-nitro-1H-isoindole-1,3(2H)-dione	-8.4 $\Delta G = -6.95$ FF = -1245.20
3	ZINC78808978		3-Nitro-N-[(1R)-1-phenylethyl]-5-(trifluoromethyl)benzamide	-8.4 $\Delta G = -7.81$ FF = -1214.69
4	ZINC387735		N-[(1R)-1-(1-Naphthyl)ethyl]acetamide	-7.6 $\Delta G = -7.29$ FF = -1258.52
5	ZINC43063883		5-Acetamido-2-methyl-N-[(1S)-1-(1-naphthyl)ethyl]benzamide	-7.3 $\Delta G = -8.41$ FF = -1253.95
6	ZINC43019010		4-Amino-N-[(1R)-1-(1-naphthyl)ethyl]benzamide	-7.3
7	ZINC1108971		2-Methyl-N-[(1R)-1-(2-naphthyl)ethyl]benzamide	-7.3
8	ZINC43063883		5-Acetamido-2-methyl-N-[(1S)-1-(1-naphthyl)ethyl]benzamide	-7.3
9	ZINC235609		5-Nitro-2-phenyl-1H-isoindole-1,3(2H)-dione	-7.2
10	ZINC95921018		3-(Hydroxyamino)-N-[(1R)-1-phenylethyl]-5-(trifluoromethyl)benzamide	-7.2
11	ZINC28952418		N-[3-(Trifluoromethyl)benzoyl]glycyl-3-[(4-methyl-3-nitrobenzyl)amino]-N-(2-methyl-2-propanyl)-L-alaninamide	-7.1
12	ZINC43019615		5-Amino-2-methyl-N-[2-(1-naphthyl)-2-propanyl]benzamide	-7.0

Table 2. continued

13	ZINC43073435		2,6-Dimethyl-N-[(1R)-1-(2-naphthyl)ethyl]benzamide	-6.9
14	ZINC13738599		2-(4-[Benzyl(ethyl)amino]butyl)-5-nitro-1H-isoindole-1,3(2H)-dione	-6.9
15	ZINC36735480		2-Methyl-N-[(1R)-1-(1-naphthyl)ethyl]benzamide	-6.8
16	ZINC43012568		5-Amino-2-methyl-N-[(1R)-1-(1-naphthyl)ethyl]benzamide	-6.8
17	ZINC8558		6-Amino-1H-benzo[de]isoquinoline-1,3(2H)-dione	-6.8
18	ZINC259008		2-Methyl-3-nitro-N-[3-(trifluoromethyl)phenyl]benzamide	-6.8
19	ZINC922210		2-({5-[4-(Diethylsulfamoyl)phenyl]-1,3,4-oxadiazol-2-yl}sulfanyl)-N-(4-ethoxyphenyl)acetamide	-6.7
20	ZINC43059603		N,2-Dimethyl-N-[(1R)-1-(1-naphthyl)ethyl]benzamide	-6.4

^aG: free energy of binding calculated by SwissDock; FF: FullFitness value calculated by SwissDock (both in kcal/mol).

3.5. Physicochemical, Cytotoxic, and Biological Properties of Identified Compounds

Full pharmacokinetic and side effect data of the five selected compounds are shown in Table 4. These data include drug-induced liver injury, human liver microsomal stability of drug against being metabolized, cytochrome P450 enzyme isoforms inhibition which leads to toxic effects, permeability through the blood–brain barrier, substrate or inhibitor of P-glycoprotein, the cell membrane protein that extracts many foreign substances from the cell, cardiotoxicity, mitochondrial toxicity, carcinogenic potential, and maximum recommended therapeutic dose of each compound.

The analysis of physicochemical properties demonstrated moderate solubility and suitable gastrointestinal (GI) absorption (Table S1) and tolerable toxicity (Table 4) for ZINC43071312. However, high doses of the compound could indicate carcinogenic potential (Table 4).

Nonsteroidal anti-inflammatory drugs (NSAIDs) are the most important class of the widely used therapeutics for the treatment of various kinds of pains and inflammations.²⁷ Gastrointestinal effects are the most serious side effects of traditional NSAIDs between various reported kinds.²⁸ NSAIDs efficiently inhibit cyclooxygenase (COX), a membrane enzyme that synthesizes prostaglandins.²⁹ COX-1 and COX-2 isoforms mainly differ in their inhibitor selectivity.³⁰ COX-2 induces inflammatory conditions and is involved in the production of

prostaglandins mediating pain and inhibition of COX-2 accounts for NSAIDs' therapeutic effects.³¹ Cyclic imides such as phthalimides with unique structural features have considerable biological activity and pharmaceutical use.³² ZINC993539 has previously been introduced as an inhibitor of COX-2 with an IC_{50} of 3.11×10^4 nM, and it is known as an anti-inflammatory and analgesic agent.³³ Based on our predictions (Table S2), ZINC993539 is moderately soluble, has high GI absorption, and, in concentrations higher than its safe dose could, cause drug-induced liver injury and cytotoxicity, and could be a carcinogenic agent (Table 4).

Drug-resistant strains of *Mycobacterium tuberculosis*, the cause of tuberculosis, have created a renewed demand to discover novel drugs to targeting this deadly pathogen.³⁴ Decaprenylphosphoryl- β -D-ribose 2'-epimerase (DprE1) is the key enzyme involved in the arabinogalactan biosynthesis that could be an essential target for inhibiting the survival of *Mycobacteria*.³⁵ Nitrobenzothiazinone could bind covalently and specifically to DprE1 and now is a preclinical candidate for combination therapy of tuberculosis.³⁶ ZINC78808978 has been described as a novel inhibitor of pyrazolopyridone class against *M. tuberculosis*.³⁷ Batt and her colleagues reported that ZINC78808978 could target DprE1, which is essential for the pathogen's viability.³⁸ Thus, this antibacterial agent may also be more investigated as a possible inhibitor for SARS-CoV-2 PLpro (Figures 7C and 8). The compound is moderately soluble, has

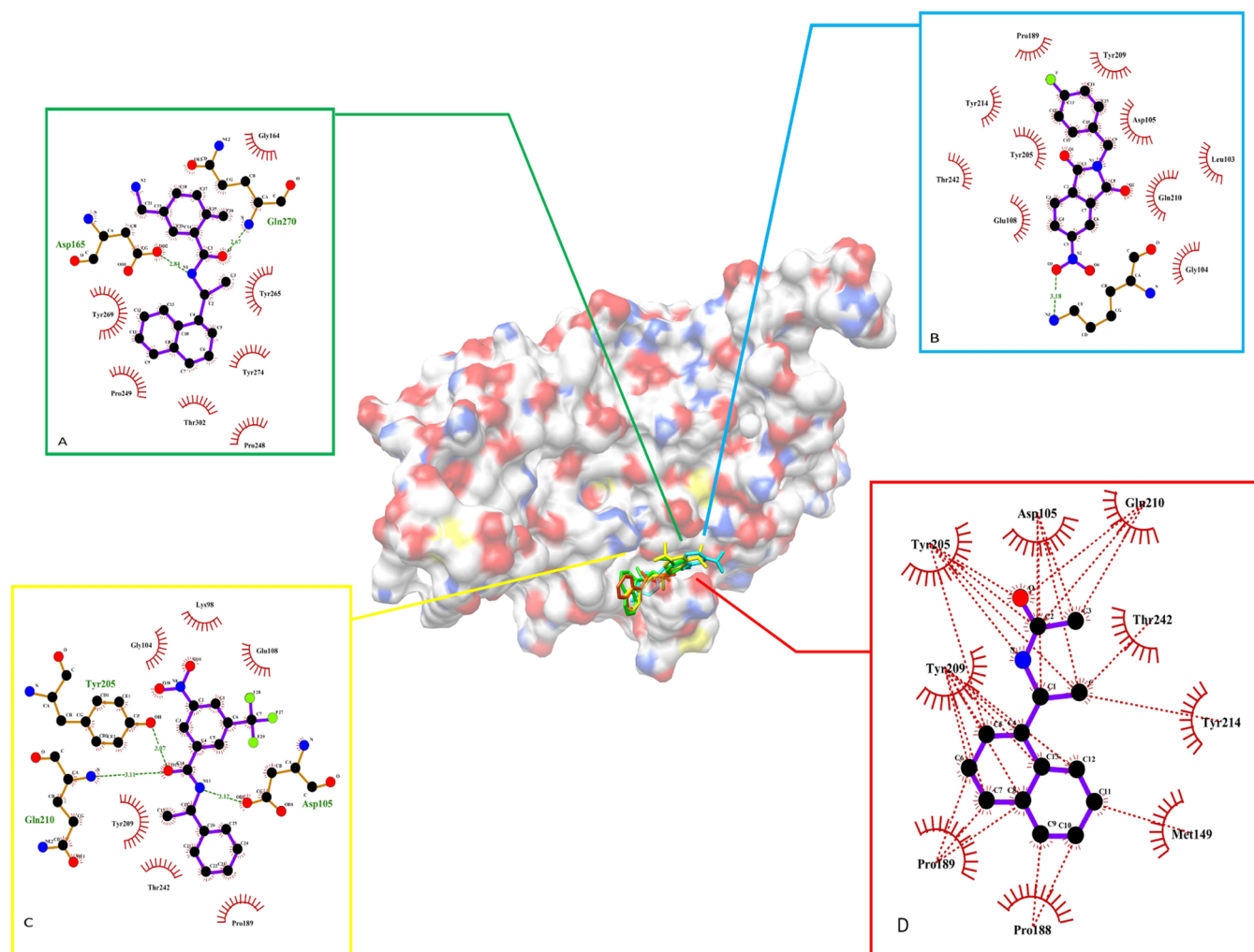


Figure 7. ZINC43071312 (green), ZINC993539 (cyan), ZINC78808978 (yellow), and ZINC387735 (red) docked into SARS-CoV-2 papain-like proteinase. 2D illustration of ZINC43071312 (A), ZINC993539 (B), ZINC78808978 (C), and ZINC387735 (D) docked to SARS-CoV-2 papain-like proteinase. For ZINC387735, all of the hydrophobic interactions with SARS-CoV-2 papain-like proteinase are shown (D).

Table 3. Binding Data for Compounds with the Lowest Interaction Energy Docked against SARS-CoV-2 PLpro after 35 ns of Molecular Dynamic Simulation, as Obtained by Two Different Docking Tools

top screened compounds with refined SARS-CoV-2 PLpro (kcal/mol)		
	affinity (Vina)	estimated ΔG (SwissDock)
ZINC43063883	-7.3	-7.96
ZINC387735	-7.2	-7.37
ZINC78808978	-7.1	-7.38
ZINC43071312	-7.0	-8.91
ZINC993539	-6.9	-6.99

high GI absorption (Table S3), and, in concentrations higher than its safe dose, could lead to drug-induced liver injury (Table 4).

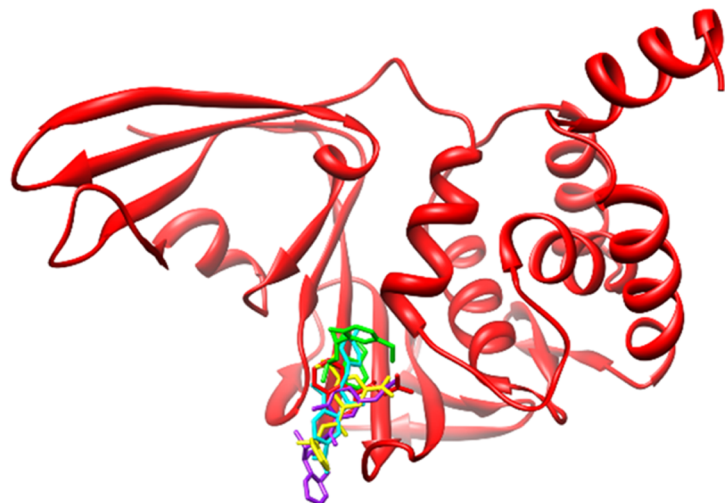
Very recently, ZINC387735 was proposed as an inhibitor for SARS-CoV-2 main proteinase through other studies,³⁹ and its structure was experimentally determined (PDB ID: SREW). Based on our docking study, this compound could interact with SARS-CoV-2 PLpro through hydrophobic interactions (Figure 7D). ZINC387735 has moderate solubility and high absorption (Table S4), but at higher concentrations of its tolerable dose that could be considered as a carcinogenic agent (Table 4).

ZINC43063883 was predicted to be a moderately soluble compound in aqueous medium, with high GI absorption (Table S5), but in higher doses than its recommended concentration that could lead to drug-induced liver injury and could be a carcinogenic agent (Table 4).

4. CONCLUSIONS

Inhibition of PLpro enzyme of SARS-CoV has been shown to efficiently inhibit the viral replication. In the current study, based on genomic homology of SARS-CoV and SARS-CoV-2, we generated optimized and dynamic simulation-refined coordinates of SARS-CoV-2 PLpro. The model was utilized in a screening procedure for identifying new inhibitory molecules against SARS-CoV-2 PLpro, based on GRL0617, a confirmed inhibitor of the enzyme from SARS-CoV. Our findings showed five compounds as potential anti-PLpro candidates, all with acceptable pharmacokinetic profiles such as fair water solubility, gastrointestinal absorption, and tolerable toxicity. Interestingly, the compounds have already been known as analgesic, anti-inflammatory, antibacterial, or antiviral drugs. Among the compounds, ZINC387735 is a recently reported inhibitor of SARS-CoV-2 PLpro. The compounds identified in this study are recommended to be further investigated for their potential as

A



B

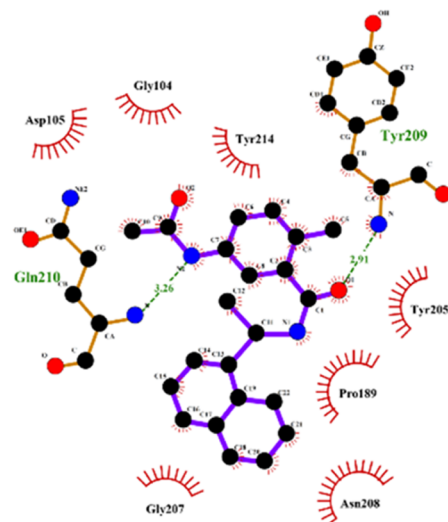


Figure 8. (A) Protein–ligand complex of ZINC43063883 (purple), ZINC387735 (red), ZINC78808978 (yellow), ZINC43071312 (green), and ZINC993539 (cyan) with papain-like protease from SARS-CoV-2 after 35 ns of molecular dynamic simulation. (B) 2D illustration of ZINC43063883 bound to SARS-CoV-2 papain-like proteinase after 35 ns of molecular dynamic simulation.

Table 4. Predicted Toxicity of Screened Compounds with Suitable Affinity for SARS-CoV-2 Papain-like Proteinase^a

	liver toxicity		metabolism						membrane transport			others			
	DILI	cytotoxicity	HLM	CYP 1A2	CYP 3A4	CYP 2D6	CYP 2C9	CYP 2C19	BBB	P-gp inhibitor	P-gp substrate	hERG blocker	MMP	AMES	MRTD (mg/day)
ZINC43071312	no	no	yes	no	no	no	no	no	yes	yes	no	no	no	yes	214
ZINC993539	yes	yes	yes	no	no	no	no	yes	no	no	no	no	no	yes	43
ZINC78808978	yes	no	yes	no	no	no	no	yes	yes	no	yes	no	no	no	525
ZINC387735	no	no	yes	no	no	no	no	no	yes	yes	no	no	no	yes	241
ZINC43063883	yes	no	no	no	no	no	yes	yes	yes	no	no	no	no	yes	768

^aDILI: drug-induced liver injury; HLM: human liver microsomal (HLM) stability of drug against being metabolized; CYP: cytochrome P450 enzyme (CYP) isoform inhibition, leading to toxic effects; BBB: permeability through the blood–brain barrier; Pgp substrates and inhibitors: substrate or inhibitor of P-glycoprotein, an essential cell membrane protein that extracts many foreign substances from the cell; hERG blocker: blocker of hERG potassium ion channel, leading to arrhythmic cardiotoxicity; MMP: mitochondrial toxicity; AMES: the mutagenic and consequently carcinogenic potential of the compound, as assessed by Ames test; MRTD: maximum recommended therapeutic dose.

suppressors of PLpro enzyme of SARS-CoV-2, with the aim of inhibiting the replication of the virus.

■ ASSOCIATED CONTENT

Supporting Information

The Supporting Information is available free of charge at <https://pubs.acs.org/doi/10.1021/acs.jproteome.0c00836>.

Physicochemical and biological properties of ZINC43071312 (Table S1); physicochemical and biological properties of ZINC993539 (Table S2); physicochemical and biological properties of ZINC78808978 (Table S3); physicochemical and biological properties of ZINC387735 (Table S4); physicochemical and biological properties of ZINC43063883 (Table S5) (PDF)

Special Issue Paper

This paper was intended for the *Proteomics in Pandemic Disease* Special Issue, published as the November 6, 2020 issue of *J. Proteome Res.* (Vol. 19, No. 11).

■ AUTHOR INFORMATION

Corresponding Author

Mostafa Jamalán – Department of Biochemistry, Abadan Faculty of Medical Sciences, Abadan 6313833177, Iran; orcid.org/0000-0002-8151-2029; Phone: +98-61-5527199; Email: mjamalanbiochem@abadanums.ac.ir, mjamalanbiochem@gmail.com

Authors

Ebrahim Barzegari – Medical Biology Research Center, Health Technology Institute, Kermanshah University of Medical Sciences, Kermanshah 6715847141, Iran
Fathollah Gholami-Borujeni – Department of Environmental Health, Mazandaran University of Medical Sciences, Mazandaran 4815733971, Iran

Complete contact information is available at: <https://pubs.acs.org/doi/10.1021/acs.jproteome.0c00836>

Notes

The authors declare no competing financial interest.

■ ABBREVIATIONS USED

COVID-19, coronavirus disease 2019; SARS-CoV, severe acute respiratory syndrome coronavirus; SARS-CoV-2, severe acute respiratory syndrome coronavirus-2; PLpro, papain-like protease; pplab, orflab polyprotein; MD, molecular dynamics; RMSD, root-mean-squared deviation; RMSF, root-mean-squared fluctuations

■ REFERENCES

- (1) (a) Lai, C.-C.; Shih, T.-P.; Ko, W.-C.; Tang, H.-J.; Hsueh, P.-R. Severe acute respiratory syndrome coronavirus 2 (SARS-CoV-2) and corona virus disease-2019 (COVID-19): the epidemic and the challenges. *Int. J. Antimicrob. Agents* **2020**, *55*, No. 105924. (b) Okba, N. M.; Müller, M. A.; Li, W.; Wang, C.; GeurtsvanKessel, C. H.; Corman, V. M.; Lamers, M. M.; Sikkema, R. S.; de Bruin, E.; Chandler, F. D.; et al. Severe acute respiratory syndrome coronavirus 2—specific antibody responses in coronavirus disease patients. *Emerging Infect. Dis.* **2020**, *26*, 1478–1488.
- (2) Acter, T.; Uddin, N.; Das, J.; Akhter, A.; Choudhury, T. R.; Kim, S. Evolution of severe acute respiratory syndrome coronavirus 2 (SARS-CoV-2) as coronavirus disease 2019 (COVID-19) pandemic: A global health emergency. *Sci. Total Environ.* **2020**, *730*, No. 138996.
- (3) Wilson, N.; Norton, A.; Young, F.; Collins, D. Airborne transmission of severe acute respiratory syndrome coronavirus-2 to healthcare workers: a narrative review. *Anaesthesia* **2020**, *75*, 1086–1095.
- (4) (a) Shah, F.; Mukherjee, P.; Gut, J.; Legac, J.; Rosenthal, P. J.; Tekwani, B. L.; Avery, M. A. Identification of novel malarial cysteine protease inhibitors using structure-based virtual screening of a focused cysteine protease inhibitor library. *J. Chem. Inf. Model.* **2011**, *51*, 852–864. (b) Shoichet, B. K. Virtual screening of chemical libraries. *Nature* **2004**, *432*, 862–865.
- (5) (a) Gao, F.; Ou, H.-Y.; Chen, L.-L.; Zheng, W.-X.; Zhang, C.-T. Prediction of proteinase cleavage sites in polyproteins of coronaviruses and its applications in analyzing SARS-CoV genomes. *FEBS Lett.* **2003**, *553*, 451–456. (b) Graziano, V.; McGrath, W. J.; DeGruccio, A. M.; Dunn, J. J.; Mangel, W. F. Enzymatic activity of the SARS coronavirus main proteinase dimer. *FEBS Lett.* **2006**, *580*, 2577–2583.
- (6) (a) Kamitani, W.; Huang, C.; Narayanan, K.; Lokugamage, K. G.; Makino, S. A two-pronged strategy to suppress host protein synthesis by SARS coronavirus Nsp1 protein. *Nat. Struct. Mol. Biol.* **2009**, *16*, 1134. (b) Huang, C.; Lokugamage, K. G.; Rozovics, J. M.; Narayanan, K.; Semler, B. L.; Makino, S. SARS coronavirus nsp1 protein induces template-dependent endonucleolytic cleavage of mRNAs: viral mRNAs are resistant to nsp1-induced RNA cleavage. *PLoS Pathog.* **2011**, *7*, No. e1002433.
- (7) (a) Sulea, T.; Lindner, H. A.; Purisima, E. O.; Ménard, R. Deubiquitination, a new function of the severe acute respiratory syndrome coronavirus papain-like protease? *J. Virol.* **2005**, *79*, 4550–4551. (b) Han, Y.-S.; Chang, G.-G.; Juo, C.-G.; Lee, H.-J.; Yeh, S.-H.; Hsu, J. T.-A.; Chen, X. Papain-like protease 2 (PLP2) from severe acute respiratory syndrome coronavirus (SARS-CoV): expression, purification, characterization, and inhibition. *Biochemistry* **2005**, *44*, 10349–10359. (c) Barretto, N.; Jukneliene, D.; Ratia, K.; Chen, Z.; Mesecar, A. D.; Baker, S. C. The papain-like protease of severe acute respiratory syndrome coronavirus has deubiquitinating activity. *J. Virol.* **2005**, *79*, 15189–15198.
- (8) (a) Chou, C.-Y.; Chien, C.-H.; Han, Y.-S.; Prebanda, M. T.; Hsieh, H.-P.; Turk, B.; Chang, G.-G.; Chen, X. Thiopurine analogues inhibit papain-like protease of severe acute respiratory syndrome coronavirus. *Biochem. Pharmacol.* **2008**, *75*, 1601–1609. (b) Ratia, K.; Pegan, S.; Takayama, J.; Sleeman, K.; Coughlin, M.; Baliji, S.; Chaudhuri, R.; Fu, W.; Prabhakar, B. S.; Johnson, M. E.; et al. A noncovalent class of papain-like protease/deubiquitinase inhibitors blocks SARS virus replication. *Proc. Natl. Acad. Sci. U.S.A.* **2008**, *105*, 16119–16124. (c) Cheng, K.-W.; Cheng, S.-C.; Chen, W.-Y.; Lin, M.-H.; Chuang, S.-J.; Cheng, I.-H.; Sun, C.-Y.; Chou, C.-Y. Thiopurine analogs and mycophenolic acid synergistically inhibit the papain-like protease of Middle East respiratory syndrome coronavirus. *Antiviral Res.* **2015**, *115*, 9–16. (d) Báez-Santos, Y. M.; John, S. E. S.; Mesecar, A. D. The SARS-coronavirus papain-like protease: structure, function and inhibition by designed antiviral compounds. *Antiviral Res.* **2015**, *115*, 21–38. (e) Cho, J. K.; Curtis-Long, M. J.; Lee, K. H.; Kim, D. W.; Ryu, H. W.; Yuk, H. J.; Park, K. H. Geranylated flavonoids displaying SARS-CoV papain-like protease inhibition from the fruits of *Paulownia tomentosa*. *Bioorg. Med. Chem.* **2013**, *21*, 3051–3057.
- (9) Sievers, F.; Wilm, A.; Dineen, D.; Gibson, T. J.; Karplus, K.; Li, W.; Lopez, R.; McWilliam, H.; Remmert, M.; Söding, J.; et al. Fast, scalable generation of high-quality protein multiple sequence alignments using Clustal Omega. *Mol. Syst. Biol.* **2011**, *7*, 539.
- (10) Pettersen, E. F.; Goddard, T. D.; Huang, C. C.; Couch, G. S.; Greenblatt, D. M.; Meng, E. C.; Ferrin, T. E. UCSF Chimera—a visualization system for exploratory research and analysis. *J. Comput. Chem.* **2004**, *25*, 1605–1612.
- (11) Van Der Spoel, D.; Lindahl, E.; Hess, B.; Groenhof, G.; Mark, A. E.; Berendsen, H. J. GROMACS: fast, flexible, and free. *J. Comput. Chem.* **2005**, *26*, 1701–1718.
- (12) Simmonett, A. C.; Pickard, F. C.; Schaefer, H. F., III; Brooks, B. R. An efficient algorithm for multipole energies and derivatives based on spherical harmonics and extensions to particle mesh Ewald. *J. Chem. Phys.* **2014**, *140*, No. 184101.
- (13) Bajusz, D.; Rácz, A.; Héberger, K. Why is Tanimoto index an appropriate choice for fingerprint-based similarity calculations? *J. Cheminf.* **2015**, *7*, No. 20.
- (14) Trott, O.; Olson, A. J. AutoDock Vina: improving the speed and accuracy of docking with a new scoring function, efficient optimization, and multithreading. *J. Comput. Chem.* **2010**, *31*, 455–461.
- (15) Morris, G. M.; Huey, R.; Lindstrom, W.; Sanner, M. F.; Belew, R. K.; Goodsell, D. S.; Olson, A. J. AutoDock4 and AutoDockTools4: Automated docking with selective receptor flexibility. *J. Comput. Chem.* **2009**, *30*, 2785–2791.
- (16) Grosdidier, A.; Zoete, V.; Michielin, O. SwissDock, a protein-small molecule docking web service based on EADock DSS. *Nucleic Acids Res.* **2011**, *39*, W270–W277.
- (17) Humphrey, W.; Dalke, A.; Schulten, K. VMD: visual molecular dynamics. *J. Mol. Graphics* **1996**, *14*, 33–38.
- (18) DeLano, W. L. Pymol: An open-source molecular graphics tool. *CCP4 Newsletter on Protein Crystallography* **2002**, *40*, 82–92.
- (19) Wallace, A. C.; Laskowski, R. A.; Thornton, J. M. LIGPLOT: a program to generate schematic diagrams of protein-ligand interactions. *Protein Eng., Des. Sel.* **1995**, *8*, 127–134.
- (20) Robert, X.; Gouet, P. Deciphering key features in protein structures with the new ENDscript server. *Nucleic Acids Res.* **2014**, *42*, W320–W324.
- (21) Pence, H. E.; Williams, A. ChemSpider: an online chemical information resource. *J. Chem. Educ.* **2010**, *87*, 1123–1124.
- (22) Daina, A.; Michielin, O.; Zoete, V. SwissADME: a free web tool to evaluate pharmacokinetics, drug-likeness and medicinal chemistry friendliness of small molecules. *Sci. Rep.* **2017**, *7*, No. 42717.
- (23) Schyman, P.; Liu, R.; Desai, V.; Wallqvist, A. vNN web server for ADMET predictions. *Front. Pharmacol.* **2017**, *8*, No. 889.
- (24) Lee, H.; Lei, H.; Santarsiero, B. D.; Gatuz, J. L.; Cao, S.; Rice, A. J.; Patel, K.; Szyplinski, M. Z.; Ojeda, I.; Ghosh, A. K.; Johnson, M. E. Inhibitor recognition specificity of MERS-CoV papain-like protease may differ from that of SARS-CoV. *ACS Chem. Biol.* **2015**, *10*, 1456–1465.
- (25) Borgio, J. F.; Alsuwat, H. S.; Al Otaibi, W. M.; Ibrahim, A. M.; Almandil, N. B.; Al Asoom, L. I.; Salahuddin, M.; Kamaraj, B.; AbdulAzeez, S. State-of-the-art tools unveil potent drug targets amongst clinically approved drugs to inhibit helicase in SARS-CoV-2. *Arch. Med. Sci.* **2020**, *16*, 508.
- (26) Chang, M. W.; Ayeni, C.; Breuer, S.; Torbett, B. E. Virtual screening for HIV protease inhibitors: a comparison of AutoDock 4 and Vina. *PLoS One* **2010**, *5*, No. e11955.
- (27) Fiorucci, S.; Meli, R.; Bucci, M.; Cirino, G. Dual inhibitors of cyclooxygenase and 5-lipoxygenase. A new avenue in anti-inflammatory therapy? *Biochem. Pharmacol.* **2001**, *62*, 1433–1438.

(28) Rainsford, K. Profile and mechanisms of gastrointestinal and other side effects of nonsteroidal anti-inflammatory drugs (NSAIDs). *Am. J. Med.* **1999**, *107*, 27–35.

(29) Rao, P.; Knaus, E. E. Evolution of nonsteroidal anti-inflammatory drugs (NSAIDs): cyclooxygenase (COX) inhibition and beyond. *J. Pharm. Pharm. Sci.* **2008**, *11*, 81s–110s.

(30) Pairet, M.; Engelhardt, G. Distinct isoforms (COX-1 and COX-2) of cyclooxygenase: possible physiological and therapeutic implications. *Fundam. Clin. Pharmacol.* **1996**, *10*, 1–15.

(31) Koehne, C.-H.; Dubois, R. N. In COX-2 Inhibition and Colorectal Cancer. In *Seminars in Oncology*; Elsevier, 2004; pp 12–21.

(32) Noguchi, T.; Shimazawa, R.; Nagasawa, K.; Hashimoto, Y. Thalidomide and its analogues as cyclooxygenase inhibitors. *Bioorg. Med. Chem. Lett.* **2002**, *12*, 1043–1046.

(33) Alanazi, A. M.; El-Azab, A. S.; Al-Suwaidan, I. A.; ElTahir, K. E. H.; Asiri, Y. A.; Abdel-Aziz, N. I.; Alaa, A.-M. Structure-based design of phthalimide derivatives as potential cyclooxygenase-2 (COX-2) inhibitors: anti-inflammatory and analgesic activities. *Eur. J. Med. Chem.* **2015**, *92*, 115–123.

(34) Zumla, A.; Nahid, P.; Cole, S. T. Advances in the development of new tuberculosis drugs and treatment regimens. *Nat. Rev. Drug Discovery* **2013**, *12*, 388–404.

(35) Riccardi, G.; Pasca, M. R.; Chiarelli, L. R.; Manina, G.; Mattevi, A.; Binda, C. The DprE1 enzyme, one of the most vulnerable targets of *Mycobacterium tuberculosis*. *Appl. Microbiol. Biotechnol.* **2013**, *97*, 8841–8848.

(36) Wang, F.; Sambandan, D.; Halder, R.; Wang, J.; Batt, S. M.; Weinrick, B.; Ahmad, I.; Yang, P.; Zhang, Y.; Kim, J.; et al. Identification of a small molecule with activity against drug-resistant and persistent tuberculosis. *Proc. Natl. Acad. Sci. U.S.A.* **2013**, *110*, E2510–E2517.

(37) Panda, M.; Ramachandran, S.; Ramachandran, V.; Shirude, P. S.; Humnabadkar, V.; Nagalapur, K.; Sharma, S.; Kaur, P.; Guptha, S.; Narayan, A.; et al. Discovery of pyrazolopyridones as a novel class of noncovalent DprE1 inhibitor with potent anti-mycobacterial activity. *J. Med. Chem.* **2014**, *57*, 4761–4771.

(38) Batt, S. M.; Jabeen, T.; Bhowruth, V.; Quill, L.; Lund, P. A.; Eggeling, L.; Alderwick, L. J.; Fütterer, K.; Besra, G. S. Structural basis of inhibition of *Mycobacterium tuberculosis* DprE1 by benzothiazinone inhibitors. *Proc. Natl. Acad. Sci. U.S.A.* **2012**, *109*, 11354–11359.

(39) Douangamath, A.; Fearon, D.; Gehrtz, P.; Krojer, T.; Lukacik, P.; Owen, C. D.; Resnick, E.; Strain-Damerell, C.; Abrányi-Balogh, P.; Brandaõ-Neto, J. Crystallographic and electrophilic fragment screening of the SARS-CoV-2 main protease. *bioRxiv* **2020**.